

## DEGRADATION OF BISPHENOL A IN AQUEOUS SOLUTION BY H<sub>2</sub>O<sub>2</sub>-ASSISTED PHOTOELECTROCATALYTIC OXIDATION

Yi-Bing Xie, Xiang-Zhong Li\*

Department of Civil and Structural Engineering,  
The Hong Kong Polytechnic University, Hong Kong, China

---

### Abstract

A series of titanium oxide (TiO<sub>2</sub>/Ti) film electrodes were prepared from titanium (Ti) metal mesh by an improved anodic oxidation process and were further modified by photochemically depositing gold (Au) on the TiO<sub>2</sub> film surface as Au-TiO<sub>2</sub>/Ti film electrodes. The morphological characteristics, crystal structure and photoelectroreactivity of both the TiO<sub>2</sub>/Ti and Au-TiO<sub>2</sub>/Ti electrodes were studied. The experiments confirmed the gold modification of TiO<sub>2</sub> film could enhance the efficiency of e<sup>-</sup>/h<sup>+</sup> separation on the TiO<sub>2</sub> conduction band and resulted in the higher photocatalytic and photoelectrocatalytic (PEC) activity under UV or visible illumination. To further enhance the TiO<sub>2</sub> PEC reaction, a reticulated vitreous carbon (RVC) electrode was applied in the same reaction system as the cathode to electrically generate H<sub>2</sub>O<sub>2</sub> in the aqueous solution. The experiments confirmed that such a H<sub>2</sub>O<sub>2</sub>-assisted TiO<sub>2</sub> PEC reaction system could achieve a much better performance of BPA degradation in aqueous solution due to an interactive effect among TiO<sub>2</sub>, Au, and H<sub>2</sub>O<sub>2</sub>. It may have good potential for application in water and wastewater treatment in the future.

*Keyword:* H<sub>2</sub>O<sub>2</sub>, Photoelectrocatalysis, RVC, TiO<sub>2</sub>

---

---

\* Corresponding author: phone: (852) 2766 6016; Fax: (852) 2334 6389; Email: cexzli@polyu.edu.hk

## 1. Introduction

In the environment, many substances either natural or synthetic chemicals have potential to interfere the hormone or endocrine systems of humans and animals even at a very low concentration [1]. A wide variety of substances, such as alkylphenolic compounds, bisphenols, dioxins, pesticides, furans, synthetic steroids, has been identified as endocrine disrupting chemicals (EDCs) and they are suspected to be able to affect the endocrine systems in various ways of causing an adverse response or disrupting their health, growth, and reproduction [2,3]. Unfortunately, these EDCs can not be degraded and removed completely by conventional biological degradation treatment. Consequently, the advanced treatment technologies are required to effectively eliminate these environmental pollutants in drinking water sources and wastewater effluents [4,5].

TiO<sub>2</sub>-based photocatalysis has been extensively studied for water and wastewater treatment because of its non-toxicity, photochemical stability, and reasonable costs. In this technique, photocatalytic (PC) oxidation of organic substances can be normally achieved with TiO<sub>2</sub> catalysts under UV illumination. Furthermore, photoelectrocatalytic (PEC) oxidation has proven to be more efficient than PC oxidation by driving the photogenerated electrons from TiO<sub>2</sub> conduction band to a counter electrode via an external circuit [6-10]. In most PEC oxidation systems, a particulate TiO<sub>2</sub> film electrode is usually used as the photoanode, while a counter electrode such as a Pt electrode is used as the cathode. Unfortunately, the role of the cathode beyond a counter electrode is usually disregarded in this kind of PEC reaction systems. Actually, some further advantages of utilizing the cathode for generating useful oxidant species such as hydrogen peroxide (H<sub>2</sub>O<sub>2</sub>) within the photoreactor could be realized, if the counter electrode is used as a functional cathode. In fact, the addition of the H<sub>2</sub>O<sub>2</sub> chemical as a sacrificial oxidant to scavenge the photo-induced TiO<sub>2</sub> conduction band electrons ( $e^-_{CB}$ ) has been proven to be beneficial for improving the efficiency of PC oxidation in a TiO<sub>2</sub> suspension system by capturing the  $e^-_{CB}$  to form the hydroxyl radical ( $\cdot OH$ ) [11,12]. Recent developments of electrochemistry have demonstrated that H<sub>2</sub>O<sub>2</sub> can be electrochemically generated on various carbon

electrodes, such as graphite or reticulated vitreous carbon (RVC) material.

In this study, while a TiO<sub>2</sub> or Au- TiO<sub>2</sub> film electrode was used as the photoanode to degrade bisphenol A (BPA) as a model EDC in aqueous solution under UV or visible illumination, a RVC electrode was applied as the cathode to generate H<sub>2</sub>O<sub>2</sub> simultaneously. Such a H<sub>2</sub>O<sub>2</sub>-assisted TiO<sub>2</sub> PEC oxidation reaction system involves several key reactions expressed as follows:



## 2. Methodology

### 2.1. Materials

BPA (2,2-bis(4-hydroxyphenyl)propane) chemical with analytical grade was purchased from Aldrich and used without further purification. Other chemicals including CH<sub>3</sub>OH, FeSO<sub>4</sub>, H<sub>2</sub>SO<sub>4</sub>, H<sub>3</sub>PO<sub>4</sub>, HF, NaF, H<sub>2</sub>O<sub>2</sub>, and H<sub>3</sub>AuCl<sub>6</sub> were also purchased from Aldrich.

Titanium mesh was purchased from Goodfellow Cambridge Ltd. (purity: 99.6 %; nominal aperture: 0.19 mm; wire diameter: 0.23 mm; wires/inch: 60 × 60; and open area: 20% twill weave) and was used as raw material to prepare TiO<sub>2</sub>/Ti and Au-TiO<sub>2</sub>/Ti mesh electrodes.

The RVC foam produced by ERG Materials and Aerospace Corporation is a new open pore foam material composed solely of vitreous carbon with large valid surface area and low electrical or fluid flow resistance (nominal density: 3%; bulk density: 1.54 g cm<sup>-3</sup>; and bulk resistivity: 0.05 ohm cm<sup>-1</sup>). In this study, the RVC foam was cut into a piece of rectangle shape (10 × 40 × 5 mm<sup>3</sup>) as the cathode.

A piece of platinum foil (surface area: 4.0 cm<sup>2</sup> and purity: 99.99%) was purchased from Sigma-Aldrich Co. Ltd and used as a counter electrode.

## 2.2. Preparation of TiO<sub>2</sub>/Ti and Au-TiO<sub>2</sub>/Ti mesh electrodes

TiO<sub>2</sub>/Ti meshes were first prepared by an improved anodic oxidation method. In which, a piece of raw Ti mesh (50 × 10 × 0.5 mm<sup>3</sup>) was firstly washed with dilute HF acid and alcohol solutions, respectively, in a supersonic cleaner and then thoroughly rinsed with distilled water; the cleaned Ti mesh was placed in 100 mL of aqueous H<sub>2</sub>SO<sub>4</sub> (1.5 M) – H<sub>3</sub>PO<sub>4</sub> (0.3 M) – H<sub>2</sub>O<sub>2</sub> (0.3 M) solution and anodized using a direct-current power supply (EPS 600, Electrophoresis Power Supply). The anodic oxidation process was conducted in two stages. In the first stage, the galvanostatic anodic oxidation with a constant current density of 60 mA cm<sup>-2</sup> was maintained until a designated anode-to-cathode voltage of 180 V was reached. In the second stage, the potentiostatic anodic oxidation with a constant voltage of 180 V was kept along with a gradually decreased current density from 60 mA cm<sup>-2</sup> to 12 mA cm<sup>-2</sup>. The whole anodic oxidation process lasted for about 30 min. Subsequently, this fresh TiO<sub>2</sub>/Ti mesh was further electrolyzed in a NaF (0.03 M) – HF (0.03 M) – H<sub>2</sub>O<sub>2</sub> (0.3 M) solution to remove some coexisting three-valence-state titanium oxides at a constant voltage of 80 V and a current density of 60 mA cm<sup>-2</sup> for 5 min. After rinsed with distilled water and dried in an oven at 378 K for 4 h, a product TiO<sub>2</sub>/Ti mesh was obtained.

The Au-TiO<sub>2</sub>/Ti meshes were also prepared using the above TiO<sub>2</sub>/Ti mesh by photoreduction of gold ion with the following procedure: the anodized TiO<sub>2</sub>/Ti mesh was placed in a cylindrical quartz cell containing 15 mL of a mixture solution (0.01 mM HAuCl<sub>4</sub>, 0.25 M CH<sub>3</sub>OH) with pH 3.2. The above solution was continuously aerated using nitrogen gas and irradiated by an 8-W middle-pressure mercury lamp for 6 h. During the photoreduction reaction, Au<sup>3+</sup> was mostly reduced to Au along with thimbleful Au<sup>2+</sup> and Au<sup>+</sup>, and deposited on the surface of TiO<sub>2</sub>/Ti mesh, in which methanol acted as a hole-scavenger to accelerate the reaction rate. The resulting Au-TiO<sub>2</sub>/Ti mesh was washed with distilled water and dried in the oven at 378 K for 24 h.

## 2.3. Characterization of TiO<sub>2</sub>/Ti and Au-TiO<sub>2</sub>/Ti mesh electrodes

To study the surface morphology, average pore size, pore distribution and metal

elements composition of the prepared TiO<sub>2</sub>/Ti and Au-TiO<sub>2</sub>/Ti meshes, scanning electron microscope (SEM LEO Stereoscan 440) equipped with an energy dispersive X-ray (EDX) analyzer was used.

To determine the crystal phase composition, X-ray diffraction (XRD) measurement was carried out using a diffractometer (Philips PW3020) fitted with a graphite monochromator, in which an accelerating voltage of 40 kV and a current of 30 mA were applied to produce Cu K $\alpha$  radiation at a wavelength of 0.15418 nm, and the samples were scanned at a step size of 0.05° and a counting time of 1 s per step in the range of  $2\theta = 10-90^\circ$ .

#### *2.4. Photoreactor setup and experimental procedures*

A bench-scale photo-electro-reactor system was used in this study and its configuration is shown in Fig 1, which is a cylindrical quartz cell with three-electrode configuration. The TiO<sub>2</sub>/Ti or Au-TiO<sub>2</sub>/Ti electrode was placed at the lower position of the reactor as the photoanode to receive light irradiation from bottom and the RVC or Pt electrode was placed at one side of cell wall nearby an air diffuser as the cathode. In addition, a saturated calomel electrode (SCE) was used as the reference electrode. A 8-W medium-pressure mercury lamp (LZC-UVA-365) was used as a UV light source (power: 8 W; light intensity: 0.68 mW cm<sup>-2</sup>; main emission: 365 nm) and a high-pressure sodium vapor lamp was used as a visible light source (power: 110 W; light intensity: 48.9 mW cm<sup>-2</sup>; emission: 450–650 nm). The electrical potential and current applied on the electrodes were regulated by a potentiostat-galvanostat. In all experiments, the H<sub>2</sub>O<sub>2</sub> generation on the RVC electrode was controlled with an electrical current rather than a potential.

[Fig. 1]

Aqueous BPA solution was prepared with an initial concentration of 11.2 mg L<sup>-1</sup> and 0.01 M Na<sub>2</sub>SO<sub>4</sub> as supporting electrolyte to increase its conductivity similar to that of sewage in Hong Kong. 30 mL of such a BPA solution was used in each experiment.

When the oxidation experiments were conducted, air was continuously aerated into the solution at a flow rate of  $120 \text{ mL min}^{-1}$ . The initial pH value was found to be 6.17 and was not controlled during the reaction. The samples were collected from the reaction solution at regular intervals for analyses.

### 2.5. Analytical methods

BPA concentration was determined by high performance liquid chromatograph, which includes a high pressure pump (Spectrasystem HPLC P4000), a UV detector (UV 6000LP), and an auto sampler (AS3000), in which an Atlantis d-C18 column ( $150 \times 4.6 \text{ mm}$  inner diameter,  $5 \mu\text{m}$  beads) was employed with a mobile phase of acetonitrile/water (7/3, v/v) at a flow rate of  $0.8 \text{ mL min}^{-1}$  and BPA concentration was determined at 278 nm by the UV detector.

The dissolved organic carbon (DOC) concentration was determined by a total organic carbon (TOC) analyzer (Shimadzu TOC-5000A). The  $\text{H}_2\text{O}_2$  concentration was determined according to the spectrum absorption of the  $\text{H}_2\text{O}_2$  and  $\text{K}_2\text{Ti}(\text{C}_2\text{O}_4)_3$  in 2 M  $\text{H}_2\text{SO}_4$  solution at 397 nm by using a UV-VIS spectrophotometer (Spectronic, GENISIS-2) [13].

## 3. Results and discussion

### 3.1. SEM and EDX analyses

To study the surface morphology of the  $\text{TiO}_2$  and Au- $\text{TiO}_2$  films, SEM measurements were performed and their SEM images are shown in Fig. 2. It can be seen that both types of films had smooth surfaces with similar micro-sized porous structures. Actually, as  $\text{TiO}_2$  was formed by anodic oxidation, the  $\text{TiO}_2$  film was firmly distributed on the surface of the Ti mesh with a good strength. The mean size of individual micropores was determined to be about 260 nm (see Fig. 2A). In the anodic oxidation process, titanium metal ( $\text{Ti}^0$ ) could be initially oxidized into different titanium oxides with a mixture of valence states such as  $\text{Ti}^{3+}$  as  $\text{Ti}_2\text{O}_3$  and  $\text{Ti}^{4+}$  as  $\text{TiO}_2$ , depending on the electrical potential applied and also the characteristics of electrolyte in the acidic solution [14]. At a high electrical potential of 180 V,  $\text{TiO}_2$  could be mainly

formed by electrolytic oxidation reaction along with oxygen molecules generated by electrolyzing  $\text{H}_2\text{O}$  ( $2\text{H}_2\text{O} - 4\text{e}^- \rightarrow \text{O}_2 + 4\text{H}^+$ ). Moreover, there also exists an equilibrium reaction between the anodic oxidation reaction to form  $\text{TiO}_2$  ( $\text{Ti} + 2\text{H}_2\text{O} \rightarrow \text{TiO}_2 + 4\text{H}^+$ ) and the electrolytic dissolution reaction to release titanium ions from the  $\text{TiO}_2$  film into the bulk solution ( $\text{TiO}_2 + 6\text{HF} \rightarrow [\text{TiF}_6]^{2-} + 2\text{H}_2\text{O} + 2\text{H}^+$  or  $\text{TiO}_2 + \text{H}_2\text{O} + \text{H}^+ \rightarrow [\text{Ti}(\text{OH})_3]^+$ ). During the high-voltage anodization, the thermal energy dissipation in the barrier oxide layer became considerably insufficient in the reaction electrolytes. Significant increase of the microstrain stress would cause the electrical breakdown of barrier oxide layer and form small cracks and veins among the crystallites formed in the sparking discharge region. As a result, a  $\text{TiO}_2$  film with a microporous structure could be gradually formed on the Ti metal surface. Due to much more excessive oxides production at titanium metal-oxide interface than  $\text{TiO}_2$  dissolution at the pore bottom of oxide-electrolyte interface, only interconnected  $\text{TiO}_2$  thick-film with microporous structure could be obtained finally [15]. Moreover, Fig. 2B showed clearly that a lot of well-distributed particulates appeared on the surface of Au- $\text{TiO}_2$  film, those are attributed to the gold particulates deposited on the  $\text{TiO}_2$  layer as clusters. Due to the existence of these gold particulates, the surface of Au- $\text{TiO}_2/\text{Ti}$  mesh became much rougher than that of pure  $\text{TiO}_2/\text{Ti}$  mesh. It might be beneficial to improve its adsorption ability. The SEM image also showed that these gold particulates have a broad range of size (10-100 nm) and well spread out both outside and inside the microspores.

[Fig. 2]

Furthermore, both the  $\text{TiO}_2/\text{Ti}$  and Au- $\text{TiO}_2/\text{Ti}$  mesh electrodes were analyzed by EDX and the results about the elemental composition of two samples are shown in Fig. 3. It can be seen that while the  $\text{TiO}_2$  mesh showed two main peaks of Ti element at 4.51 and 4.92 keV (as Ti  $\text{K}\alpha$  line) and one peak of O element at 0.52 keV (as O  $\text{K}\alpha$  line), the Au- $\text{TiO}_2/\text{Ti}$  mesh showed other five new peaks attributable to Au element at 1.75, 2.18, 2.93 (as Au  $\text{M}\alpha$  line), 9.71 (as Au  $\text{L}\alpha$  line), and 11.52 keV (as Au  $\text{L}\beta$  line), respectively [16]. These results confirmed the Au deposition on the  $\text{TiO}_2$  film by the photoreduction

reaction. In addition, an approximate ratio of Au/Ti was estimated by the peak area of different metal elements to be about 0.76 at% (atom percent of Au in TiO<sub>2</sub>).

[Fig. 3]

### 3.2. XRD analysis

To study the crystal structure of catalysts, three meshes (Ti, TiO<sub>2</sub>/Ti and Au-TiO<sub>2</sub>) were examined by XRD and their XRD patterns are shown in Fig. 4. The results showed two characteristic diffraction peaks of anatase occurred at  $2\theta = 25.4^\circ$  for (101) plane and  $2\theta = 48.1^\circ$  for (200) plane, respectively, and demonstrated both the TiO<sub>2</sub>/Ti and Au-TiO<sub>2</sub>/Ti meshes are only predominated by anatase with a similar crystal structure. Since the anodic oxidation process was conducted in two stages (galvanostatic anodization and potentiostatical anodization), it is believed that the galvanostatic anodization with a high current density and a low voltage is initially to oxidize titanium into titanium oxides and to form amorphous TiO<sub>2</sub>, then the subsequent potentiostatical anodization at a high voltage and a low current density led to crystallize TiO<sub>2</sub> into a more regular phase structure and eventually to complete crystallization. It is believed that the crystalline transformation from amorphous to anatase is associated with local exothermic heat caused by the spark discharge, since the anodic voltage of 180 V is much higher than the sparking voltage of TiO<sub>2</sub> (about 80 to 100 V). Therefore, this anodic oxidation process can achieve the complete crystallization of TiO<sub>2</sub> without calcination. Meanwhile, the crystalline transformation from anatase to rutile has also been restrained because H<sub>3</sub>PO<sub>4</sub> electrolyte could well contribute thermal transmittance in the local sparking region of TiO<sub>2</sub> barrier layer [17]. Therefore, the different conditions used in the anodic oxidation process such as electrical potential, current density, and electrolyte composition would influence the crystallization degree and microstructure of TiO<sub>2</sub> film significantly.

[Fig. 4]

### 3.3. Voltammetry property

To investigate the electrochemical properties of the TiO<sub>2</sub>/Ti and Au-TiO<sub>2</sub>/Ti meshes, a set of cyclic voltammetry measurements was carried out in a standard three-electrode assembly, which consists of a TiO<sub>2</sub>/Ti or Au-TiO<sub>2</sub>/Ti electrode as the working electrode, a Pt foil as the counter electrode and a saturated calomel reference electrode. In the tests, the linear sweep voltammetry was recorded at a scanning step of 10 mV s<sup>-1</sup> and the results of cyclic voltammetry are shown in Fig. 5. It was found that the critical potential of water oxidation was determined to be 2.84 V vs. SCE for the TiO<sub>2</sub>/Ti electrode and 1.82 V vs. SCE for the Au-TiO<sub>2</sub>/Ti electrode, respectively. Both potentials are more positive than the theoretical value ( $2\text{H}_2\text{O} - 4\text{e}^- \rightarrow \text{O}_2 + 4\text{H}^+$ ,  $E^0 = 0.987$  V vs. SCE), due to an effect of over-potential on the TiO<sub>2</sub>/Ti and Au-TiO<sub>2</sub>/Ti semiconductor electrodes. Since the Au-TiO<sub>2</sub>/Ti electrode had a relatively lower critical potential than the TiO<sub>2</sub>/Ti electrode, it might indicate that the Au-TiO<sub>2</sub>/Ti electrode could conduct the H<sub>2</sub>O cleaving reaction more accessibly to produce oxygen than the TiO<sub>2</sub>/Ti electrode. Furthermore, the Au-TiO<sub>2</sub>/Ti electrode generated a higher polarization current than the TiO<sub>2</sub>/Ti electrode at the same anodic potentials. It means that the more feasible electron-transfer process could occur on the Au-TiO<sub>2</sub>/Ti electrode, which could ultimately promote the electro-hole pair ( $\text{e}^-/\text{h}^+$ ) separation during the PEC reaction.

[Fig. 5]

### 3.4. H<sub>2</sub>O<sub>2</sub> generation on the RVC cathode

H<sub>2</sub>O<sub>2</sub> can be electrically generated from oxygen in aqueous solution by an electrochemical reduction reaction on the carbon cathode.



If it is assumed that this electrochemical reaction achieved an efficiency of 100 %, a theoretical amount of the H<sub>2</sub>O<sub>2</sub> generation could be calculated using the following two equations:

$$Q = I \times t \quad (6)$$

Where  $Q$  is total electron coulombs amount (C);  $t$  is reaction time (s) and  $I$  is current intensity (A).

$$Q = 2n \times N_A \times e = 2n \times (6.02 \times 10^{23}) \times (1.60 \times 10^{-19}) \quad (7)$$

Where  $n$  is the moles of electrogenerated  $H_2O_2$  (mol);  $N_A$  is Avogadro's number ( $6.02 \times 10^{23}$  molecules/mole); and  $e$  is electron charge ( $1.60 \times 10^{-19}$  C).

According the above equations, it can be calculated that when the current intensity on the RVC cathode was 0.5, 1.0, and 1.5 mA, the theoretical cumulative concentration of  $H_2O_2$  in 30 mL solution after 180 min. reaction was 0.905, 1.809, and 2.714 mM, respectively.

In general, such a  $H_2O_2$  electrogeneration reaction mainly relies on several factors including the electrode material, applied current density, the oxygen coverage on the cathode, pH, and electrolyte concentration. To investigate the interactive effects between  $H_2O_2$  electrogeneration and consumption reaction, two sets of experiments were carried out in aqueous solution with and without BPA, respectively.

The first set of experiments using Pt and RVC electrodes was conducted in aqueous solution without BPA under the same experimental conditions by applying different current density (0.5, 1.0, and 1.5 mA). Each experiment lasted for 240 min and the cumulative  $H_2O_2$  concentration ( $C_{H_2O_2}$ ) in aqueous solution vs. electrolyzing time ( $t$ ) was obtained and the results are shown in Fig. 6 (curves a, b and c). The experiments demonstrated that the  $C_{H_2O_2}$  in the solution increased quickly along with the electrolyzing time in the initial period and further gradually increased with a lower growth rate to eventually reach its maximum value. It can be concluded that the higher current density applied achieved the  $C_{H_2O_2}$  in the solution. To determine a relationship between  $C_{H_2O_2}$  and  $t$ , it is assumed that the generation rate of  $H_2O_2$  concentration is proportional to the current intensity ( $I$ ) applied on the cathode as the first-order reaction ( $\frac{dc}{dt} = kI$ ) and an exponential model,  $C = aI(1 - e^{-kt})$ , was applied to fit the experimental data. It can be seen that the proposed model fitted the data very well in all experiments. If the apparent current efficiency (ACE) under this experimental

condition is defined as  $ACE = \Delta(\text{H}_2\text{O}_2)_{\text{experimental value}} / \Delta(\text{H}_2\text{O}_2)_{\text{theoretical value}} \times 100 \%$ , ACE can be determined to be 35.5 %, 34.8 % and 35.8 %, for the applied current intensity at 0.5, 1.0, and 1.5 mA (corresponding current density = 40, 80 and 120  $\mu\text{A cm}^{-2}$  on the RVC cathode), respectively.

The second set of experiments using  $\text{TiO}_2$  and RVC electrodes was conducted in aqueous BPA solution under UV illumination to investigate the  $\text{H}_2\text{O}_2$  concentration during BPA degradation reaction. Each experiment also lasted for 240 min and the experimental results about  $\text{H}_2\text{O}_2$  concentration vs. experimental time were obtained and also fitted by the exponential model as shown in Fig. 6 (curves d, e, and f). The results showed that  $\text{H}_2\text{O}_2$  concentration with existence of BPA degradation reaction under UV illumination was significantly lower than that without BPA. It can be explained that  $\text{H}_2\text{O}_2$  was actively involved in the PEC reaction and its consumption rate was much faster than its decomposition rate in aqueous  $\text{Na}_2\text{SO}_4$  solution without BPA.

[Fig. 6]

### 3.5. PC/PEC degradation of BPA under UV illumination with $\text{TiO}_2/\text{Ti}$

To better understand the BPA degradation reaction in such a  $\text{H}_2\text{O}_2$ -assisted  $\text{TiO}_2$  PEC reaction system, the BPA degradation experiments were conducted in aqueous solution under UV illumination, in which the  $\text{TiO}_2/\text{Ti}$  electrode was used as the photoanode and the RVC electrode was used as the cathode. The first set of experiments was performed by applying different current intensity from 0 to 1.5 mA and results are presented in Fig. 7A. The experiment of BPA degradation with zero current intensity ( $I = 0$  mA) demonstrated a slow reaction with a BPA removal of only 10% after 180 min. Actually, such a reaction was equivalent to the  $\text{TiO}_2$  PC reaction without  $\text{H}_2\text{O}_2$  at all. Other experiments with current intensity from 0.2 to 1.5 mA showed a better performance and BPA removal was achieved by 65-99%. These results demonstrated that the electrogenerated  $\text{H}_2\text{O}_2$  from the RVC cathode could improve the BPA degradation significantly under this experimental condition. In fact, at the lower range of current intensity ( $I < 0.5$  mA),  $\text{H}_2\text{O}_2$  plays a role of scavenging electrons from the

TiO<sub>2</sub>-CB and also generates hydroxyl radical ( $\text{H}_2\text{O}_2 + \text{e}^-_{\text{CB}} \rightarrow \text{OH}^- + \cdot\text{OH}$ ) to enhance BPA degradation reaction. However, at the higher range of current intensity ( $I = 1.0\text{-}1.5$  mA), corresponding electrical potential on the TiO<sub>2</sub>/Ti anode (up to 7.0 V) was much higher than a critical potential of 2.84 V to execute the electro-oxidation of water and BPA on the TiO<sub>2</sub> anode. In the meantime, the TiO<sub>2</sub> film on the TiO<sub>2</sub>/Ti electrode could also dissolve as titanium ions into the bulk solution by a low-voltage anodization corrosion process. A relationship between the applied potential and current intensity of TiO<sub>2</sub>/Ti electrode is shown in Fig. 7B. Furthermore, although H<sub>2</sub>O<sub>2</sub> may generate hydroxyl radical directly under UV illumination as  $\text{H}_2\text{O}_2 + \text{UV} \rightarrow 2\cdot\text{OH}$ , it is believed that such a photolysis process is insignificant under UV-A illumination.

[Fig. 7]

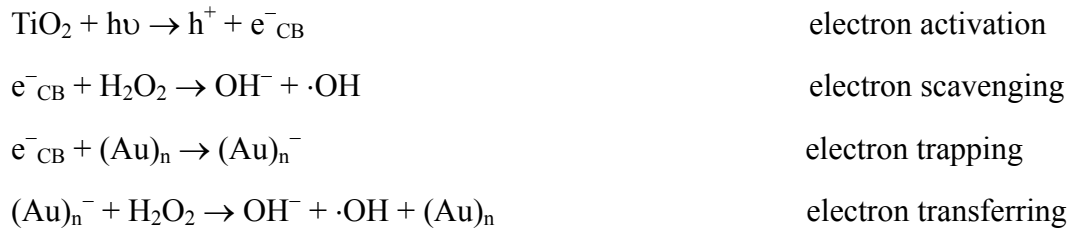
### 3.6. PC/PEC degradation of BPA under UV/visible illumination with Au-TiO<sub>2</sub>/Ti

Many research papers have reported that noble metal surface modification could improve the reaction activity of TiO<sub>2</sub> catalyst [18,19]. In this study, the gold-modified TiO<sub>2</sub> catalyst (Au-TiO<sub>2</sub>/Ti electrode) was applied for PC/PEC degradation of BPA under UV/visible light illumination. The experimental results are compared with the performance using the TiO<sub>2</sub>/Ti electrodes. The PC oxidation results are shown in Fig. 8. The results showed that BPA degradation under UV illumination was achieved by 13.2 % using the TiO<sub>2</sub>/Ti electrode and by 22.9% using the Au-TiO<sub>2</sub>/Ti electrode for 180 min. This result indicates that the gold modification on the TiO<sub>2</sub> surface can enhance the PC activity of TiO<sub>2</sub> under UV illumination significantly. However, the results also demonstrated that BPA degradation under visible light illumination was achieved by less than 5% after 180 min in both cases, although the Au-TiO<sub>2</sub>/Ti electrode performed slightly better than the TiO<sub>2</sub>/Ti electrode. These results indicate the gold modification only resulted in a slight improvement in the PC activity of TiO<sub>2</sub> under visible light illumination. Such a weak photoactivity of Au-TiO<sub>2</sub> is ascribed to gold nanoparticulates rather than TiO<sub>2</sub>, which is mostly associated with sensitive surface plasmon response of metallic gold clusters by visible photon energy excitation

[20]. These results indicate that the gold deposition on TiO<sub>2</sub> surface may not photosensitize TiO<sub>2</sub> catalyst from UV response to the visible light range effectively, but can enhance its photocatalytic activity under UV illumination significantly.

[Fig. 8]

The results of PEC oxidation under UV illumination at a current intensity of  $I = 1.5$  mA are shown in Fig. 9. It can be seen that the Au-TiO<sub>2</sub>/Ti anode achieved better BPA degradation together with either Pt cathode without H<sub>2</sub>O<sub>2</sub> generation or the RVC cathode with H<sub>2</sub>O<sub>2</sub> generation than the TiO<sub>2</sub>/Ti anode. These results confirmed that the BPA degradation reaction in aqueous solution can be enhanced by both the gold modification and also H<sub>2</sub>O<sub>2</sub> electrogeneration, but H<sub>2</sub>O<sub>2</sub> involvement is more significant than the gold modification. In such a H<sub>2</sub>O<sub>2</sub>-assisted Au-TiO<sub>2</sub> PEC reaction system, some key reactions are identified as follows:



Since the PC/PEC reaction highly relies on the efficiency of  $e^-/h^+$  separation. The  $e^-_{\text{CB}}$  transfer rate on the TiO<sub>2</sub> conduction band can be regarded as a rate-determining step for the whole reaction. Due to a more negative Fermi level of TiO<sub>2</sub> semiconductor than gold nanoparticulates, a Schottky junction could be formed by Fermi level equilibration shift for Au-TiO<sub>2</sub> composite, which causes a space-charge layer at the gold metal–TiO<sub>2</sub> interfacial region. So the gold metal and TiO<sub>2</sub> phases are in a good electronic communication [21]. Once  $e^-/h^+$  is generated under UV excitation,  $e^-_{\text{CB}}$  could smoothly inject into Au clusters. Most importantly, the determinant electron transfer process could subsequently occur from gold clusters to electron-acceptors (such as peroxides or dissolved oxygen). The formation of a Schottky barrier would

lead to a decrease of  $e^-/h^+$  recombination as well as an increase of the quantum yields. Accordingly, gold deposition on  $TiO_2$  surface enhances PC/PEC reaction by indirectly accelerating the transfer from  $e^-_{CB}$  to  $H_2O_2$ . Regarding the pure  $TiO_2$  semiconductor, the  $e^-/h^+$  separation occurs in the heterogeneous interface by electron transfer from  $e^-_{CB}$  to  $H_2O_2$ . Such a process exhibits less effective in comparison with the electron-injection process in the internal surface between  $TiO_2$  and gold clusters. Therefore, in addition to  $TiO_2$  electron transfer driven by external electronic field, gold deposition also plays an important role in the dynamic separation of such photogenerated charge carriers. However, once a gold loading exceeds its optimum value such as Au/Ti atom fraction percent  $> 5\%$ , negatively charged gold clusters would attract  $TiO_2$  holes and subsequently recombine with  $e^-_{CB}$ . In this case, gold deposits become recombination centers and have a detrimental effect on the PC and PEC activity [22].

[Fig. 9]

#### **4. Conclusions**

Well-crystallized  $TiO_2/Ti$  film electrodes with a microporous structure were successfully prepared by a direct anodization process at a high voltage and further modified by gold deposition on the  $TiO_2$  surface to form Au- $TiO_2/Ti$  film electrodes. The experiments confirmed the gold modified  $TiO_2$  film could enhance the efficiency of  $e^-/h^+$  separation on the  $TiO_2$  conduction band and resulted in higher PC and PEC activity under UV or visible illumination. In the meantime,  $H_2O_2$  could be effectively and also continuously generated in the  $TiO_2$  PEC reaction system, when a RVC electrode was used as the cathode. It has been confirmed that such a  $H_2O_2$ -assisted  $TiO_2$  PEC reaction system could achieve a much better performance of BPA degradation in aqueous solution with potential for application in water and wastewater treatment.

#### **Acknowledgement**

We would like to thank the Research Grant Committee of the Hong Kong Government for financial support of this work (PolyU5148/03E).

## References

- [1] E. Harries, T. Runnalls, E. Hill, C.A. Harris, S. Maddix, J.P. Sumpter, C.R. Tyler, Development of a reproductive performance test for endocrine disrupting chemicals using pair-breeding fathead minnows (*Pimephales promelas*), *Environ. Sci. Technol.* 34 (2000) 3003-3011.
- [2] A. Menditto, L. Turrio-Baldassarri, Environmental and biological monitoring of endocrine disrupting chemicals, *Chemosphere* 39 (1999) 1301-1307.
- [3] A. Mantovani, Hazard identification and risk assessment of endocrine disrupting chemicals with regard to developmental effects, *Toxicology*, 181-182 (2002) 367-370.
- [4] T. Nakashima, Y. Ohko, D.A. Tryk, A. Fujishima, Decomposition of endocrine-disrupting chemicals in water by use of TiO<sub>2</sub> photocatalysts immobilized on polytetrafluoroethylene mesh sheets, *J. Photochem. Photobiol. A: Chem.* 151 (2002) 207-212.
- [5] H. Katsumata, S. Kawabe, S. Kaneco, T. Suzuki, K. Ohta, Degradation of bisphenol A in water by the photo-Fenton reaction, *J. Photochem. Photobiol. A: Chem.* 162 (2004) 297-305.
- [6] K. Vinodgopal, S. Hotchandani, P.V. Kamat, Electrochemically assisted photocatalysis - TiO<sub>2</sub> particulate film electrodes for photocatalytic degradation of 4-chlorophenoL, *J. Phys. Chem.* 97 (1993) 9040-9044.
- [7] J.A. Byrne, B.R. Eggins, Photoelectrochemistry of oxalate on particulate titanium dioxide, *J. Electroanal. Chem.* 457 (1998) 61-72.
- [8] R.J. Candal, W.A. Zeltner, M.A. Anderson, Effect of ph an applied potential on photocurrent and oxidation rate of saline solutions of formic acid in a photoelectrocatalytic reactor, *Environ. Sci. Technol.* 34 (2000) 3443-3451.
- [9] M.E. Calvo, R.J. Candal, S.A. Bilmes, Photooxidation of organic mixtures on biased TiO<sub>2</sub> films, *Environ. Sci. Technol.* 35 (2001) 4132-4138.

- [10] J.J. Sene, W.A. Zeltner, M.A. Anderson, Fundamental photoelectrocatalytic and electrophoretic mobility studies of TiO<sub>2</sub> and v-doped TiO<sub>2</sub> thin-film electrode materials, *J. Phys. Chem. B* 107 (2003) 1597-1603.
- [11] J.M. Friedrich, C. Ponce-De-Leon, G.W. Reade, F.C. Walsh, Reticulated vitreous carbon as an electrode material, *J. Electroanal. Chem.* 561 (2004) 203-217.
- [12] R.R. Ozer, J.L. Ferry, Investigation of the photocatalytic activity of TiO<sub>2</sub>-polyoxometalate systems, *Environ. Sci. Technol.* 35 (2001) 3242-3246.
- [13] R.M. Sellers, Spectrophotometric determination of hydrogen peroxide using potassium titanium oxalate, *Analyst.* 105 (1980) 950-954.
- [14] C.E.B. Marino, E.M. de Oliveira, R.C. Rocha-Filho, S.R. Biaggio, On the stability of thin-anodic-oxide films of titanium in acid phosphoric media, *Corros. Sci.* 43 (2001) 1465-1476.
- [15] J.S. Choi, R.B. Wehrspohn, J. Lee, U. Gosele, Anodization of nanoimprinted titanium: a comparison with formation of porous alumina, *Electrochim. Acta* 49 (2004) 2645-2652.
- [16] A. Orlov, D.A. Jefferson, N. Macleod, R.M. Lambert, Photocatalytic properties of TiO<sub>2</sub> modified with gold nanoparticles in the degradation of 4-chlorophenol in aqueous solution, *Catal. Lett.* 92 (2004) 41-47.
- [17] M. Iwasaki, Y. Iwasaki, H. Tada, S. Ito, One-pot process for anodic oxide films of titanium with high photocatalytic activity, *Mater. Trans.* 45 (2004) 1607-1612.
- [18] K. Zakrzewska, M. Radecka, A. Kruk, W. Osuch, Noble metal/titanium dioxide nanocermets for photoelectrochemical applications, *Solid State Ionics* 157 (2003) 349-356.
- [19] F. Boccuzzi, A. Chiorino, M. Manzoli, D. Andreeva, T. Tabakova, L. Ilievab, V. Iadakiev, Gold, silver and copper catalysts supported on TiO<sub>2</sub> for pure hydrogen production, *Catal. Today* 75 (2002) 169-175.
- [20] I.M. Arabatzis, T. Stergiopoulos, D. Andreeva, S. Kitova, S.G. Neophytides, P. Falaras, Characterization and photocatalytic activity of Au/TiO<sub>2</sub> thin films for azo-dye degradation, *J. Catal.* 220 (2003) 127-135.
- [21] V. Subramanian, E. Wolf, P.V. Kamat, Semiconductor-Metal Composite

- Nanostructures. To What extent metal nanoparticles (Au, Pt, Ir) improve the photocatalytic activity of TiO<sub>2</sub> films, *J. Phys. Chem. B* 105 (2001) 11439-11446.
- [22] O. Carp, C.L. Huisman, A. Reller, Photoinduced reactivity of titanium dioxide, *Prog. Solid State Chem.* 32 (2004) 33-177.

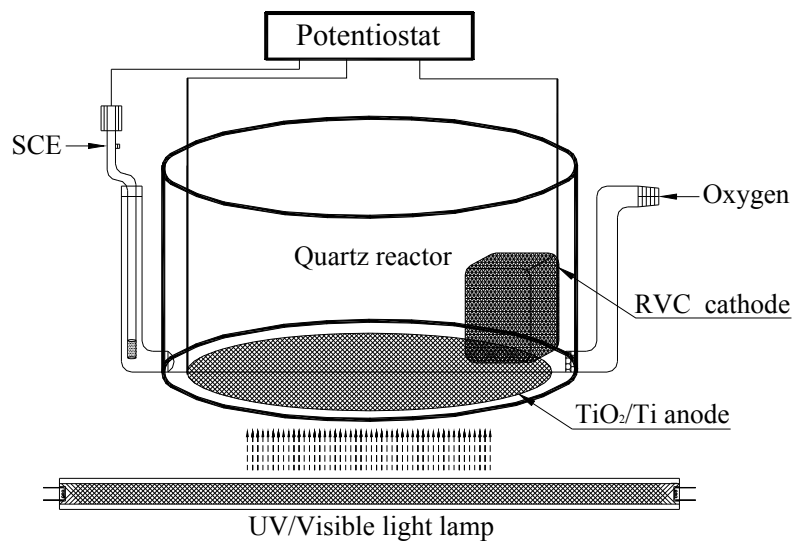


Fig. 1. Schematic diagram of the photoreaction equipment.

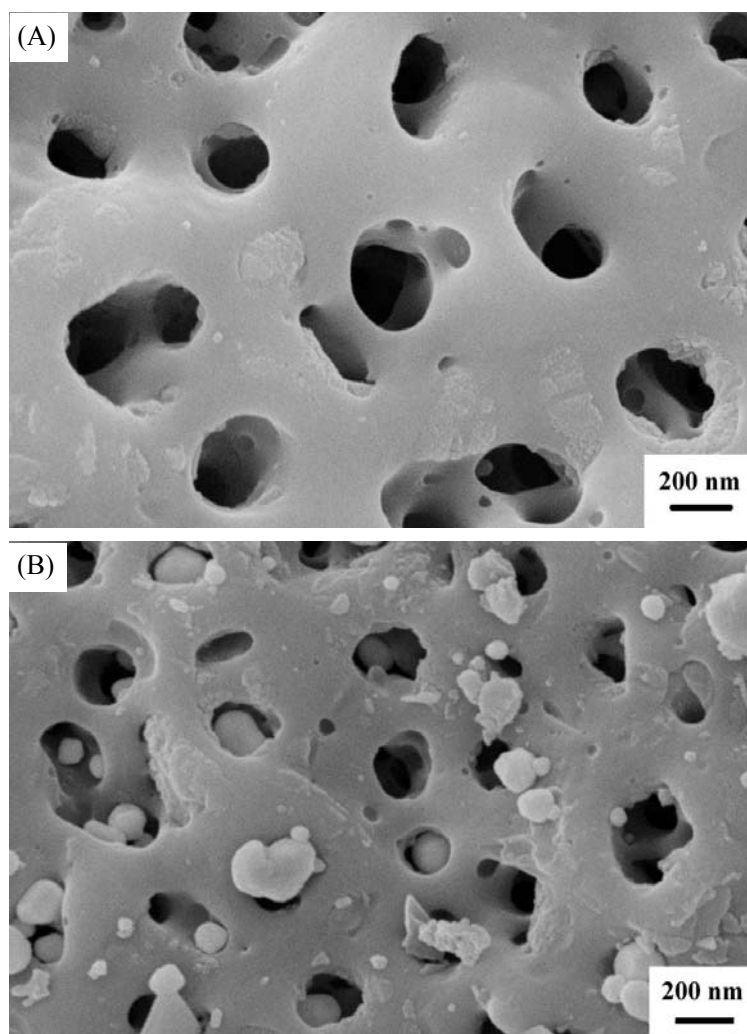


Fig. 2. SEM images of (A) TiO<sub>2</sub>/Ti and (B) Au-TiO<sub>2</sub>/Ti mesh electrodes.

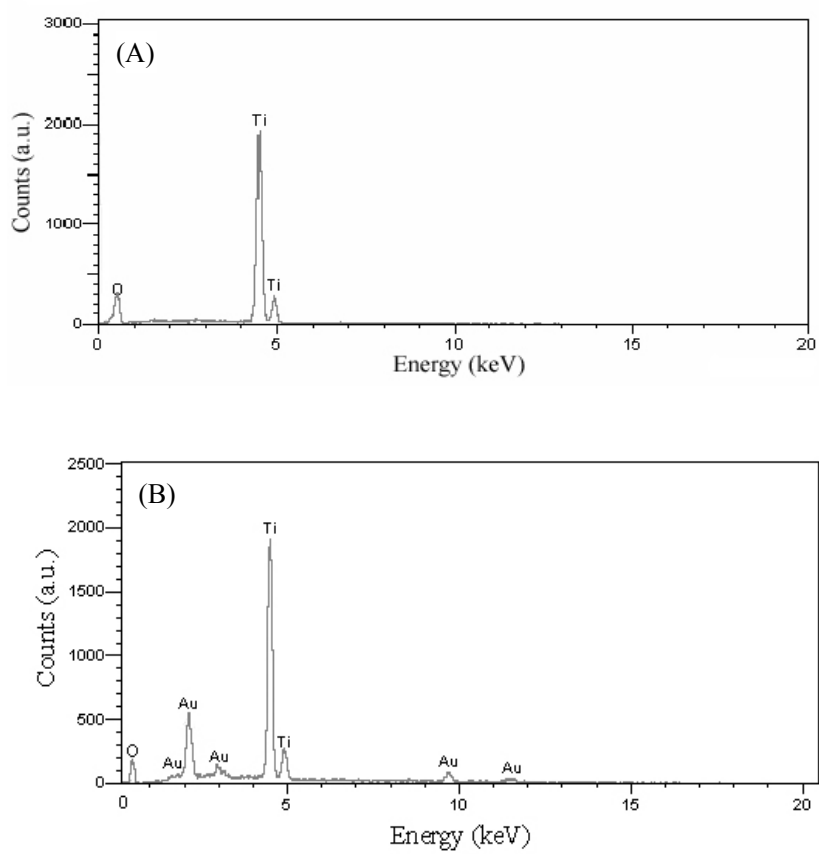


Fig. 3. Energy dispersive X-ray spectra of (A) TiO<sub>2</sub>/Ti and (B) Au-TiO<sub>2</sub>/Ti mesh electrodes.

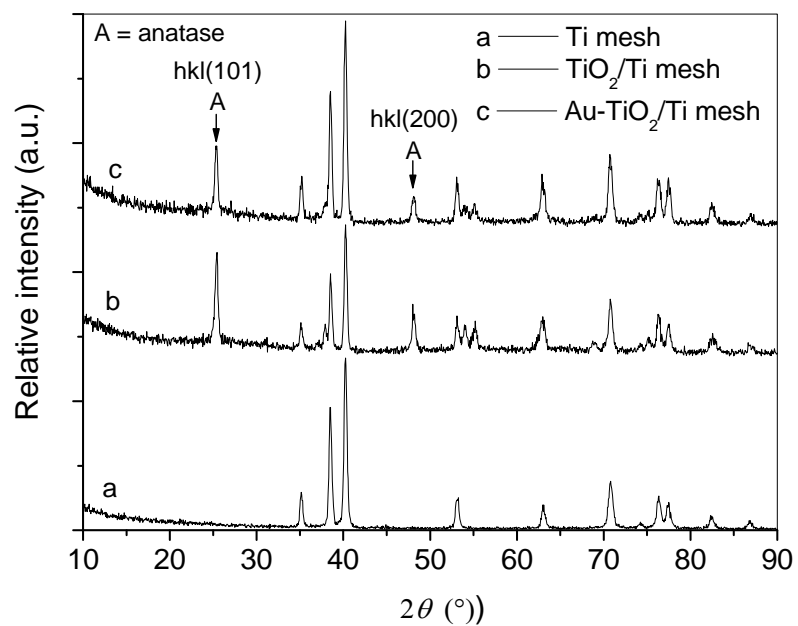


Fig. 4. XRD patterns of the  $\text{TiO}_2/\text{Ti}$  and  $\text{Au-TiO}_2/\text{Ti}$  mesh electrodes.

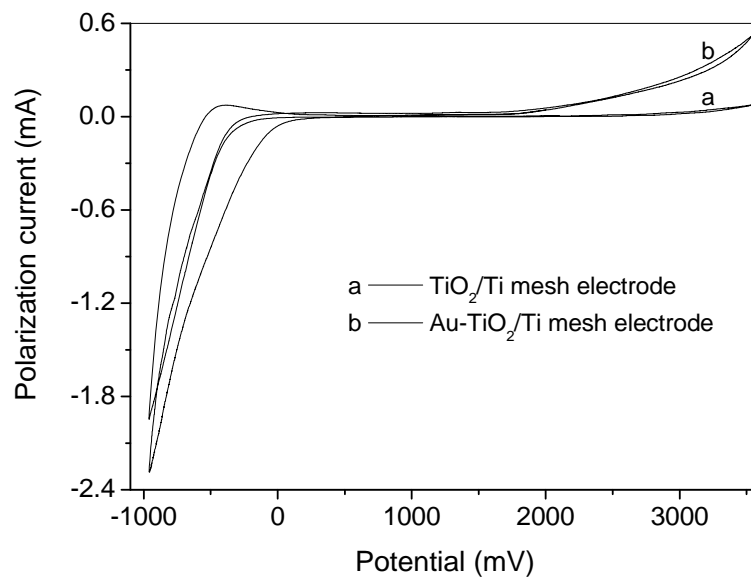


Fig. 5. Cyclic voltammety curves of TiO<sub>2</sub>/Ti and Au-TiO<sub>2</sub>/Ti mesh electrodes in 0.01 M Na<sub>2</sub>SO<sub>4</sub> electrolyte solution.

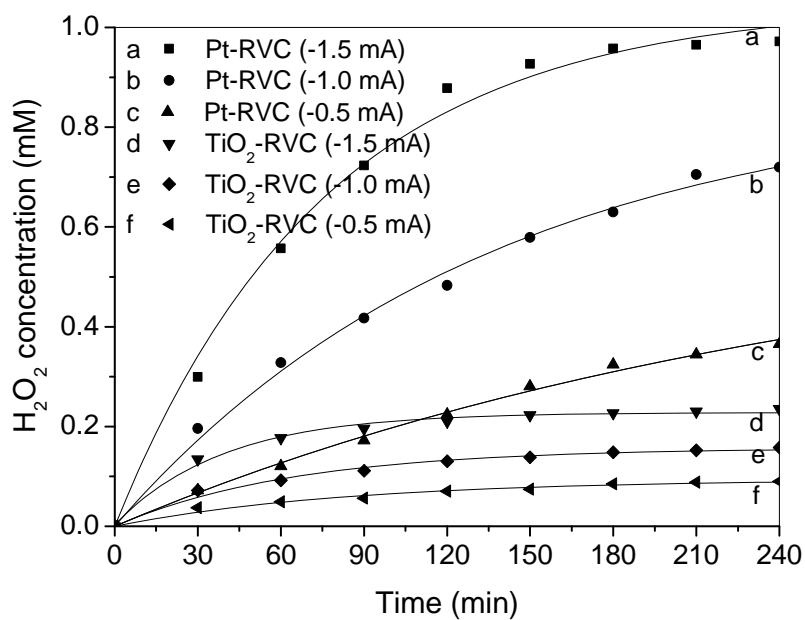


Fig. 6. H<sub>2</sub>O<sub>2</sub> cumulating concentration in Pt-RVC electrochemical system for oxygen reduction reaction (curve a, b and c) and TiO<sub>2</sub>-RVC photoelectrocatalysis system for BPA degradation reaction (curve d, e and f) under different cathode current condition (RVC cathode as a working cathode, Pt or TiO<sub>2</sub>/Ti as a count electrode and SCE as a reference electrode).

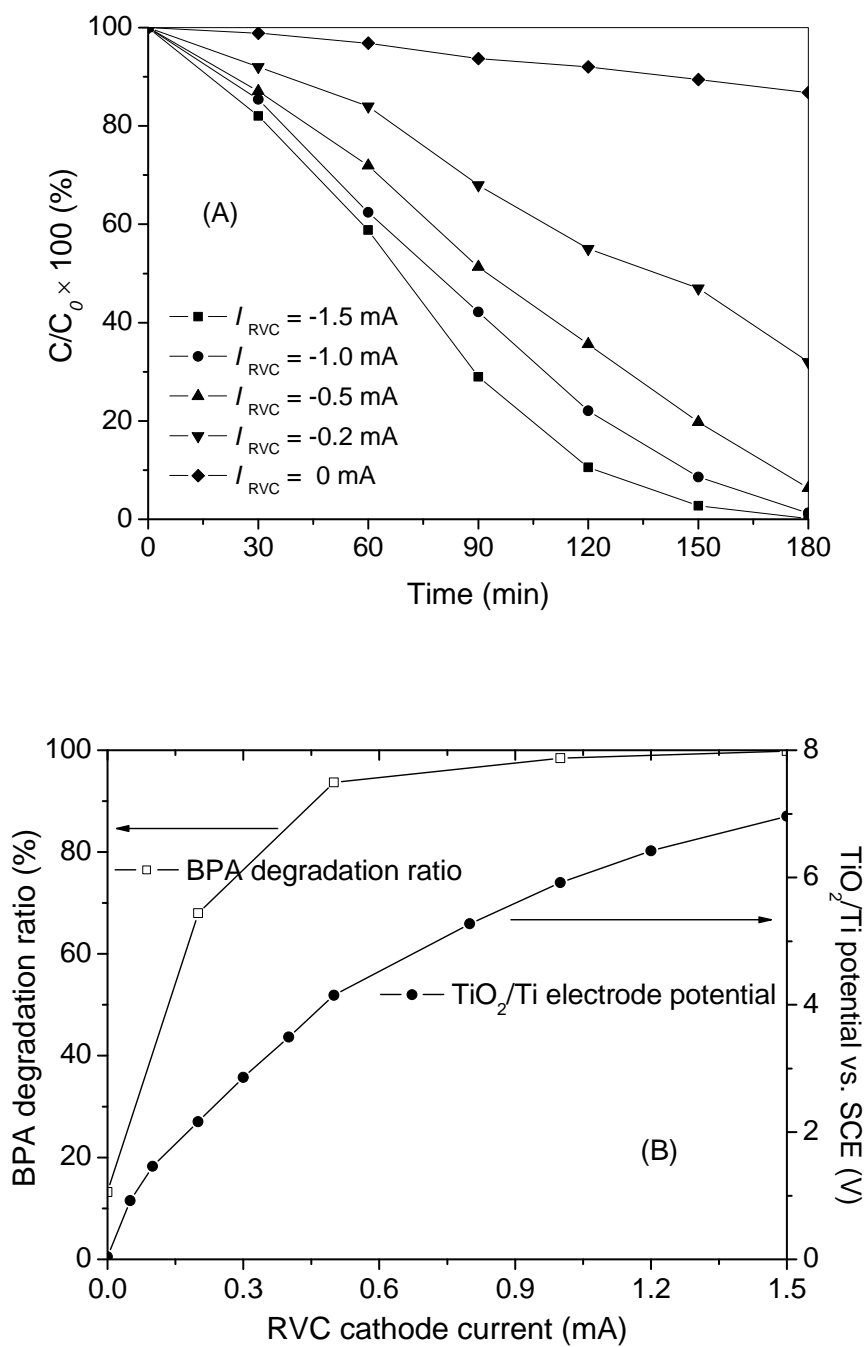


Fig. 7. (A) BPA degradation ratio and (B)  $TiO_2/Ti$  electrode potential under different RVC cathode current intensity in  $TiO_2/Ti$ -RVC photoelectrocatalytic reaction system.

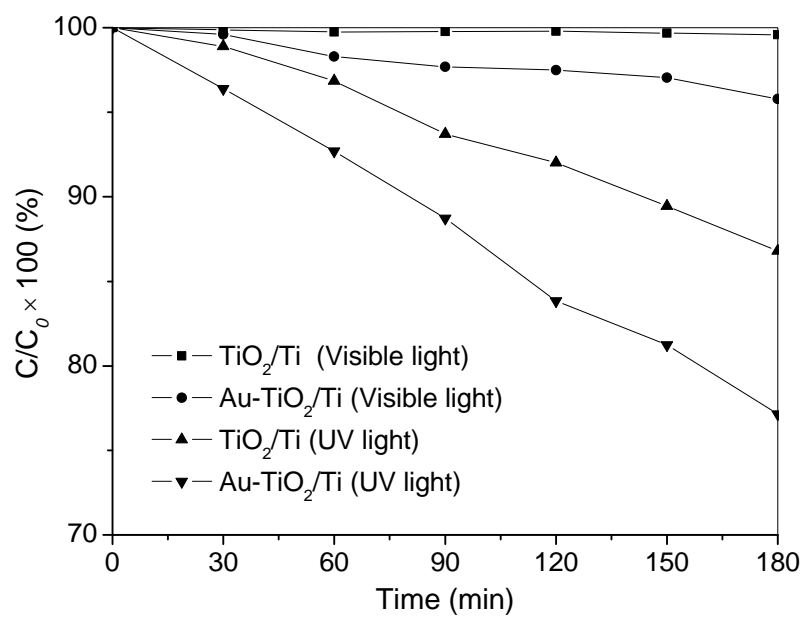


Fig. 8. Photocatalytic degradation of BPA by  $\text{TiO}_2/\text{Ti}$  and  $\text{Au-TiO}_2/\text{Ti}$  mesh electrode under UV or visible light illumination.

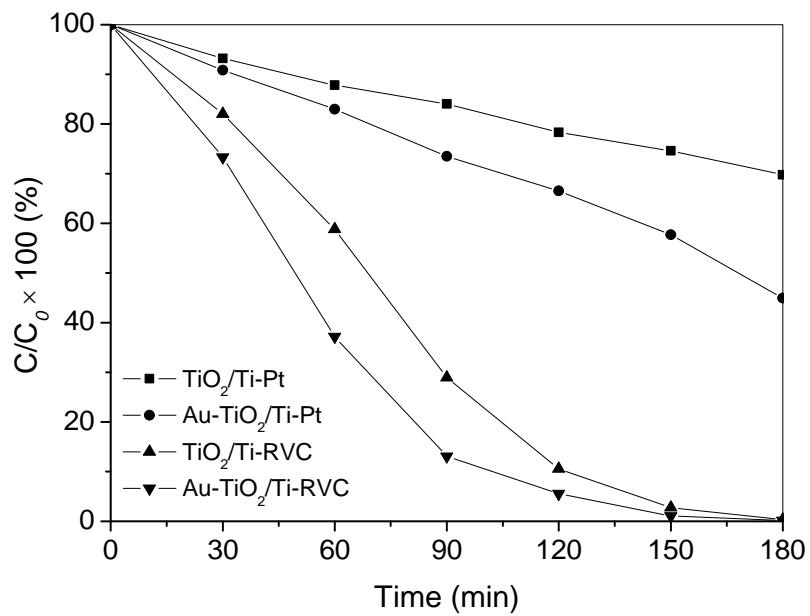


Fig. 9. Photoelectrocatalytic reaction efficiency by using different electrode pair under UV illumination (Current intensity = 1.5 mA).